The Eurasia Proceedings of Science, Technology, Engineering & Mathematics (EPSTEM)
ISSN: 2602-3199

The Eurasia Proceedings of Science, Technology, Engineering & Mathematics (EPSTEM), 2022

Volume 21, Pages 506-516

IConTES 2022: International Conference on Technology, Engineering and Science

Water Remediation from Recalcitrant Pollution Using the Galvano-Fenton Process: A Modeling Approach of the Hydroxyl Radical Generation and the Energy Efficiency

Kaouther KERBOUA
Higher School of Industrial Technologies

Naoufel HADDOUR
Laboratoire Ampère, Ecole Centrale de Lyon

Intissar GASMI
Badji Mokhtar - Annaba University

Oualid HAMDAOUI
King Saud University

Abstract: The hydroxyl radical is the most powerful oxidant after fluorine, and is the key reactant of the advanced oxidation processes AOP. Monitoring the kinetics of formation and reaction of this short life species is one of the challenging tasks from an experimental point of view. Thus, modelling is suggested to be one efficient tool for a comprehensive and predictive study of AOPs, particularly the Galvano-Fenton process. In the present study, mathematical modelling is used to describe the kinetics of hydroxyl radical $HO^{\bullet}$ generation and organic substrate RO degradation within the Galvano-Fenton process, based on the spontaneous galvanic corrosion of iron waste and in situ ferrous ion catalyst generation. A range of typical absolute kinetic constants of 10^6 à 10^{10} $M^{-1}.s^{-1}$ is considered to characterize the attack of RO species by $HO^{\bullet}$. Phenol is presented as a model pollutant for a total mineralization model. The numerical simulations demonstration a quasi-linear evolution of hydroxyl radical production during the first stage of the Galvano-Fenton process. A comparison of the Galvano-Fenton process with the classic Fenton in terms of kinetics, and electro-Fenton in terms of energetic performance, revealed that the spontaneous galvanic generation of ferrous ions in the Galvano-Fenton process leads to a higher rate of the reaction a higher instantaneous concentration of ferric ions accompanying the release of hydroxyl radicals and hence a better oxidation efficiency, as well as a positive energy balance. A particular attention was given to the ratio of the degradation efficiency to the released energy.

Keywords: Advanced oxidation, Spontaneous corrosion, Kinetics, Chemical mechanism, Energy efficiency.

Introduction

The non-selective and highly reactive $^{\bullet}$OH radical (Haag 1992) is a chemical species of great interest in terms of degradation of organic pollutants and recalcitrant contaminants in aqueous solutions (Madhavan, Grieser, and Ashokkumar 2010; Pawar and Gawande 2015). Fenton mechanism though known since the thirties of the last century (Haber and Weiss 1932; Liochev and Fridovich 2002), remains an up to date technique still studied by several researchers (Shokri 2018; Xu, Chu, and Graham 2014). The Fenton reaction plays fundamental roles in in vivo and advanced oxidation processes (AOPs) (De Laat and Gallard 1999; De Laat and Le 2006; De Laat, Truong Le, and Legube 2004; Madhavan, Grieser, and Ashokkumar 2010), with both of its classic or modified forms included in the so-called “Fenton-based techniques”. The most challenging aspects of Fenton mechanism

concerns the resolution of one of the major limitations of classic Fenton process (Fe^{2+}/H_2O_2), which is the need to use stoichiometric amount of the catalyst, Fe(II) (Andreozzi, Apuzzo, and Marotta 2000). Indeed, the decomposition of hydrogen peroxide in the Fenton reaction is catalyzed by Fe(II). The Fe(II) oxidizes to Fe(III), while the hydroxyl radical is produced as illustrated in Figure 1a. Fe(III) is expected to regenerate Fe(II) through the reaction with hydrogen peroxide. However, this reaction is known to be very slow, owing to the formation of intermediate non-radical species such as $Fe(HO_2)^{2+}$. Hence, the classic Fenton process needs high amounts of Fenton's reagent to generate a high enough quantity of $HO^{\bullet}$, which implies economic and environmental issues. Moreover, the formation of Fe^{3+} ions and their slow transformation into Fenton's catalyst promote the occurrence of wasting reactions, directly impacting the overall efficiency of the process (Monteil et al. 2019).

Fenton based techniques such as photo-Fenton or electro-Fenton for the treatment of wastewater were studied by several scientists such as Martins et al. (Martins et al. 2006), Tarkwa et al. (Tarkwa et al. 2019), and more recently, Lu et al. (Lu et al. 2021). These techniques use additional energy and/or chemicals to generate highly oxidizing agents, mainly hydroxyl radicals. The required energy constitutes another techno-economic limitation of the Fenton based techniques.

The fundamental idea of Galvano Fenton process is rightly keeping on the advantage of in situ production of Fenton's reagents but without consuming energy, along with insuring continuity of the process. Galvano-Fenton process was designed by coupling classic Fenton to the principle of galvanic cell, with the objective of recovering solid iron waste in form of sacrificial anode and hence produce the ferrous iron catalyst in situ. In galvanic cell, the sacrificial anode is expected to corrode spontaneously under the effect of the higher standard potential of the cathode, selected among the more noble metals (Lower, 2012). In Galvano-Fenton process, this principle is harnessed by coupling iron to copper, the iron being of lower standard redox potential (Shreir, Jarman & Burstein 1994), its corrosion produces continuously and in situ ferrous ions, which are the catalyst of the Fenton mechanism. The Galvano-Fenton process clearly presents three major technical benefits. On one hand, it does not require external energy supply and it provides a catalyst for the targeted process, which is Fenton, preventing then the need of catalyst addition, on the other hand and especially at larger scale, it would serve as ecological solution for recovering solid iron wastes.

The present paper aims to numerically assess the performance of the Galvano-Fenton process based on the simultaneous immersion of electrodes in the electrolyte and the addition of hydrogen peroxide, with particular attention to an energetic parameter, namely, the ratios of hydroxyl radical production and degradation efficiency to the released energy. The Galvano-Fenton process is investigated in terms of the degradation of a model pollutant, namely phenol, until its total mineralization. It is studied based on the kinetics of formation and transformation of ferrous and ferric ions, the free radicals' generation, and the pollutant degradation. Furthermore, energetic insights are given, particularly for the comparison of the positive and negative energy balances presented by the electro-Fenton and the Galvano-Fenton processes, relating their respective performances in terms of the generation of hydroxyl radicals and phenol's degradation.

Method

Configuration of the Modelled Process

The Galvano-Fenton process is designed by immersing a galvanic cell of iron anode (sacrificial anode) and copper cathode within an acidified electrolyte, at the pH condition allowing the formation of ferrous ions according to the Pourbaix diagram. Hydrogen peroxide is added to the electrolyte while the spontaneous corrosion of iron occurs, provoking the Fenton reaction. The process is simulated considering a corrosion current of 300 µA, determined experimentally during the preliminary test described below. The current value is equivalent to a current density of 25 $\mu A/cm^2$ reported to the active surface of the anode of 12 cm^2. The Galvano-Fenton system is modeled by combining electrochemical reactions taking place at the anode and the cathode with chemical reactions related to the Fenton mechanism occurring in the bulk liquid volume. In the presence of phenol, a detailed oxidation mechanism is proposed in Table. 2, to describe the whole evolution of the reactions occring at the electrodes and in the electrolyte.

The Fenton based mechanism is validated experimentally using blank tests, i.e., in the absence of phenol. The test consists of immersing both electrodes in the acidified electrolyte at pH 3 using sulfuric acid (mother solution concentration 0.1 N, supplied from Sigma-Aldrich), and simultaneously adding hydrogen peroxide (mother solution concentration 30% v/v, purchased from Sigma-Aldrich) in initial concentration of 0.35 mM.

The electrolyte is stirred at 200 RPM to homogenize the mixture and promote displacement of ionic species between electrodes. The kinetics of Fe(III) is monitored over time using spectrophotometric measurements of absorbance at 303 nm ($\varepsilon = 2197\ \mathrm{L.mol^{-1}.cm^{-1}}$) (Merouani et al. 2010). Each preliminary blank test lasts 20 minutes with 1 min spaced regular sampling during the first 10 minutes, and 2 min spaced withdrawals during the rest of the time. The corrosion current is determined during the same test using A zero ammeter placed between both electrodes of the galvanic cell described in Table.1. The polarization curves have been also plotted using a galvanostat-potentiostat connected to the same cell, the corrosion current has been confirmed by this method as well, through the intersection of both Tafel's lines.

Table 1. Specifications of the Galvano-Fenton cell

Parameter	Specification
Electrodes form	rectangular smooth plates
Immersed electrodes surface	6 cm^2
Electrolyte volume	100 mL
Electrodes disposition	In parallel
Electrolyte nature	Acidified water (H_2SO_4)
pH	3
Electrical connection	External wire
Ionic displacement	Aided by a magnetic stirring
Initial concentration of hydrogen peroxide (In the presence of phenol)	0.186 mM
Initial concentration of hydrogen peroxide (blank test)	0.35 mM

Numerical Modelling

Iron constitutes the sacrificial electrode, Fe oxidizes to Fe^{2+} ($E^0 = -0.44$ V vs. SHE) according to Equation 1, in Table.2. At the cathode, the most probable reaction concerns the reduction of H^+ to form H_2 ($E^0 = 0$ V vs. SHE) according to Eq.2 in Table.2, owing to the acidity of the medium. This has been proven in a previous work conducted by our research group (Gasmi et al. 2020). The kinetics related to all of the electrochemical reactions are governed by Faraday's law (Z. Ahmad 2006), given in Equation (1), and describe the evolution of the C_k concentration of the species involved in the electrochemical reactions in a function of time.

$$\frac{dC_k}{dt} = \pm\frac{i_{corr}}{nFV} \tag{1}$$

n represents the valence number; it equals 2 for reaction 1 and 1 for reaction 2. *F* is Faraday's number, which equals 96,490 C/mol. i_{corr} represents the corrosion current, while *V* constitutes the volume of the electrolyte. Table 2. Electrochemical and chemical scheme of the possible reactions occurring at the electrodes and in the electrolyte by the Galvano Fenton-based processes in the presence of phenol; k_i is the absolute reaction constant of the i^{th} reaction. Adapted from (Bray 1931; Koprivanac and Lon, 2006; De Laat and Le 2006; Machulek Jr et al., 2009).

The chemical kinetic equations describing the evolution of the chemical mechanism occurring in the electrolyte are set based on the kinetics constant reported in previous table. Each reaction can be schematized according to Equation (2).

$$\sum_{k=1}^{K} v'_{ki} X_k \rightarrow \sum_{k=1}^{K} v''_{ki} X_k \tag{2}$$

v'_{ki} is the stoichiometric coefficient related to the kth species X_k within the ith chemical reaction. The kinetics rate related to the i^{th} reaction is expressed as reported in Equation (3).

$$r_i = k_i \prod_{k=1}^{K} [C_k]^{\vartheta'_{ki}} \tag{31}$$

k_i is the kinetic constant related to the i^{th} reaction occurring in the electrolyte in the presence of phenol among the 49 reported in Table 2 and is determined at the operating temperature of 25 °C in the present study.

	i	i^{th} Reaction	k_i	Unit of k_i
Anode	1	$Fe \rightarrow Fe^{2+} + 2e^-$	-	-
Cathode	2	$2\,H^+ + 2e^- \rightarrow H_2$	-	-
	3	$Fe^{2+} + H_2O_2 \rightarrow Fe^{3+} + OH^- + HO^\bullet$	6.3×10^{-2}	$mol^{-1}.m^3.s^{-1}$
	4	$Fe^{3+} + H_2O_2 \rightarrow Fe(HO_2)^{2+} + H^+$	3.1×10^{4}	$mol^{-1}.m^3.s^{-1}$
	5	$Fe(HO_2)^{2+} + H^+ \rightarrow Fe^{3+} + H_2O_2$	1.0×10^{7}	$mol^{-1}.m^3.s^{-1}$
	6	$Fe(HO_2)^{2+} \rightarrow Fe^{2+} + HO_2^\bullet$	2.3×10^{-3}	s^{-1}
	7	$H_2O_2 + HO^\bullet \rightarrow HO_2^\bullet + H_2O$	3.3×10^{4}	$mol^{-1}.m^3.s^{-1}$
	8	$HO_2^\bullet \rightarrow O_2^{\bullet-} + H^+$	1.58×10^{5}	s^{-1}
	9	$O_2^{\bullet-} + H^+ \rightarrow HO_2^\bullet$	1.0×10^{7}	$mol^{-1}.m^3.s^{-1}$
	10	$Fe^{2+} + HO^\bullet \rightarrow Fe^{3+} + OH^-$	3.2×10^{5}	$mol^{-1}.m^3.s^{-1}$
	11	$HO_2^\bullet + Fe^{2+} + H_2O \rightarrow Fe^{3+} + H_2O_2 + OH^-$	1.2×10^{3}	$mol^{-1}.m^3.s^{-1}$
	12	$HO_2^\bullet + Fe^{3+} \rightarrow Fe^{2+} + H^+ + O_2$	3.6×10^{2}	$mol^{-1}.m^3.s^{-1}$
	13	$O_2^{\bullet-} + Fe^{2+} + 2H_2O \rightarrow Fe^{3+} + H_2O_2 + 2\,OH^-$	1.0×10^{4}	$mol^{-1}.m^3.s^{-1}$
	14	$O_2^{\bullet-} + Fe^{3+} \rightarrow Fe^{2+} + O_2$	5.0×10^{4}	$mol^{-1}.m^3.s^{-1}$
	15	$HO^\bullet + HO^\bullet \rightarrow H_2O_2$	5.2×10^{6}	$mol^{-1}.m^3.s^{-1}$
	16	$HO_2^\bullet + HO_2^\bullet \rightarrow H_2O_2 + O_2$	8.3×10^{2}	$mol^{-1}.m^3.s^{-1}$
	17	$O_2^{\bullet-} + H^+ \rightarrow HO_2^\bullet$	1.0×10^{7}	$mol^{-1}.m^3.s^{-1}$
	18	$HO^\bullet + HO_2^\bullet \rightarrow O_2 + H_2O$	7.1×10^{6}	$mol^{-1}.m^3.s^{-1}$
	19	$HO^\bullet + O_2^{\bullet-} \rightarrow O_2 + OH^-$	1.01×10^{7}	$mol^{-1}.m^3.s^{-1}$
	20	$HO_2^\bullet + O_2^{\bullet-} + H_2O \rightarrow H_2O_2 + O_2 + OH^-$	9.7×10^{4}	$mol^{-1}.m^3.s^{-1}$
	21	$HO_2^\bullet + H_2O_2 \rightarrow O_2 + HO^\bullet + H_2O$	5.0×10^{-4}	$mol^{-1}.m^3.s^{-1}$
	22	$O_2^{\bullet-} + H_2O_2 \rightarrow O_2 + HO^\bullet + OH^-$	1.3×10^{-4}	$mol^{-1}.m^3.s^{-1}$
	23	$Fe^{2+} + {SO_4}^{2-} \rightarrow FeSO_4$	2.29×10^{8}	$mol^{-1}.m^3.s^{-1}$
	24	${SO_4}^{2-} + HO^\bullet \rightarrow {SO_4}^{\bullet-} + OH^-$	1.4×10^{4}	$mol^{-1}.m^3.s^{-1}$
	25	${HSO_4}^- + HO^\bullet \rightarrow {SO_4}^{\bullet-} + H_2O$	3.5×10^{2}	$mol^{-1}.m^3.s^{-1}$
	26	${SO_4}^{\bullet-} + H_2O \rightarrow H^+ + {SO_4}^{2-} + HO^\bullet$	3.0×10^{5}	s^{-1}
Electrolyte	27	${SO_4}^{\bullet-} + OH^- \rightarrow {SO_4}^{2-} + HO^\bullet$	1.4×10^{4}	$mol^{-1}.m^3.s^{-1}$
	28	${SO_4}^{\bullet-} + H_2O_2 \rightarrow {SO_4}^{2-} + H^+ + HO_2^\bullet$	1.2×10^{4}	$mol^{-1}.m^3.s^{-1}$
	29	${SO_4}^{\bullet-} + HO_2^\bullet \rightarrow {SO_4}^{2-} + H^+ + O_2$	3.5×10^{6}	$mol^{-1}.m^3.s^{-1}$
	30	${SO_4}^{\bullet-} + Fe^{2+} \rightarrow Fe^{3+} + {SO_4}^{2-}$	3.0×10^{5}	$mol^{-1}.m^3.s^{-1}$
	31	$FeSO_4 \rightarrow Fe^{2+} + {SO_4}^{2-}$	1.0×10^{10}	s^{-1}
	32	$Fe^{3+} + H_2O \rightarrow FeOH^{2+} + H^+$	2.9×10^{7}	s^{-1}
	33	$FeOH^{2+} + H^+ \rightarrow Fe^{3+} + H_2O$	1.0×10^{7}	$mol^{-1}.m^3.s^{-1}$
	34	$FeOH^{2+} + H_2O_2 \rightarrow Fe(OH){HO_2}^{+} + H^+$	2.0×10^{3}	$mol^{-1}.m^3.s^{-1}$
	35	$Fe(OH){HO_2}^{+} + H^+ \rightarrow FeOH^{2+} + H_2O_2$	1.0×10^{7}	$mol^{-1}.m^3.s^{-1}$
	36	$Fe(OH){HO_2}^{+} \rightarrow Fe^{2+} + HO_2^\bullet + OH^-$	2.3×10^{-3}	s^{-1}
	37	$Ph + HO^\bullet \rightarrow DHCD^\bullet$	7.3×10^{6}	$mol^{-1}.m^3.s^{-1}$
	38	$DHCD^\bullet + H^+ \rightarrow Ph^\bullet + H_2O$	5.0×10^{5}	$mol^{-1}.m^3.s^{-1}$
	39	$DHCD^\bullet + O_2 \rightarrow CC + HO_2^\bullet$	1.5×10^{6}	$mol^{-1}.m^3.s^{-1}$
	40	$DHCD^\bullet + O_2 \rightarrow HQ + HO_2^\bullet$	5.0×10^{5}	$mol^{-1}.m^3.s^{-1}$
	41	$DHCD^\bullet + O_2 \rightarrow BQ + HO_2^\bullet$	5.0×10^{5}	$mol^{-1}.m^3.s^{-1}$
	42	$DHCD^\bullet + BQ \rightarrow Ph^\bullet + CC + HQ$	3.7×10^{6}	$mol^{-1}.m^3.s^{-1}$
	43	$2DHCD^\bullet \rightarrow Ph + CC$	5.0×10^{5}	$mol^{-1}.m^3.s^{-1}$
	44	$2DHCD^\bullet \rightarrow products$	5.0×10^{5}	$mol^{-1}.m^3.s^{-1}$
	45	$DHCD^\bullet + Ph^\bullet \rightarrow products$	5.0×10^{5}	$mol^{-1}.m^3.s^{-1}$
	46	$DHCD^\bullet + Ph^\bullet \rightarrow Ph + CC + HQ$	5.0×10^{5}	$mol^{-1}.m^3.s^{-1}$
	47	$Ph^\bullet + Ph^\bullet \rightarrow products$	1.0×10^{6}	$mol^{-1}.m^3.s^{-1}$
	48	$BQ + {O_2}^{\bullet-} \rightarrow HPH^\bullet + O_2$	1.0×10^{6}	$mol^{-1}.m^3.s^{-1}$
	49	$CC + HO^\bullet \rightarrow products$	1.1×10^{7}	$mol^{-1}.m^3.s^{-1}$
	50	$HQ + HO^\bullet \rightarrow products$	5.0×10^{6}	$mol^{-1}.m^3.s^{-1}$
	51	$BQ + HO^\bullet \rightarrow products$	1.2×10^{6}	$mol^{-1}.m^3.s^{-1}$

PH: phenol, C_6H_6O. DHCD•: dihydroxy cyclohexadienyl radical, $C_{12}H_{16}O_3$. PH•: phenyl radical, C_6H_5. HPH•: hydroxyphenyl radical, C_6H_4OH. CC: catechol, $C_6H_6O_2$. HQ: hydroquinone, $C_6H_6O_2$. BQ: benzoquinone $C_6H_4O_2$

The kinetics of apparition and the disappearance of a species X_k in the electrolyte is governed by Equation (4) for species involved in the electrochemical reactions:

$$\frac{d[X_k]}{dt} = \pm\frac{1}{nV}\frac{i_{corr}}{F} + \sum_{i=1}^{N}(v''_{ki} - v'_{ki})\, k_i \prod_{j=1}^{K}[X_j]^{\vartheta'_{ji}} \quad (4)$$

Equation (5) is applicable to species that are only implicated in the electrolytic reactions (Davis and Davis 2003).

$$\frac{d[X_k]}{dt} = \sum_{i=1}^{N}(v''_{ki} - v'_{ki})\, k_i \prod_{j=1}^{K}[X_j]^{\vartheta'_{ji}} \quad (5)$$

The system of non-linear differential equations derived from Equations (1) to (5) is resolved using the fourth-order Runge–Kutta algorithm on Matlab with a fixed step of 1 s. The simulation is performed over 1200 s.

Results and Discussion

Validation of the Simulation

The preliminary blank tests performed in the absence of phenol allowed the validation of the chemical mechanism combining the electrochemical reactions occurring at the electrodes and the chemical reactions related to Fenton mechanism, occurring in the electrolyte, without considering the presence of an organic substrate susceptible to be attacked by the hydroxyl radicals. The validation is based on the experimental quantification of Fe(III) species, and the comparison with the predicted trend retrieved numerically.

The kinetics of Fe(III) was assessed experimentally using the Fricke dosimetry principle. Fig.1 reports the experimental results for the evolution of the concentration of Fe(III) species, as well as the simulation results, returning the total concentration of species containing Fe at its +3 oxidation state, and the concentration of each one of these species. The concentrations of Fe(II) species obtained by simulation are reported as well. The simulation curve of Fe(III) concentration obtained based on no cathodic regeneration of Fe^{2+}, the reactivity of sulfate ions and emergence of ferric complexes within the electrolyte solution is well correlated with the experimental results and shows a correlation coefficient based on Bravais-Pearson formula (Artusi, Verderio, and Marubini 2002) of 93.5%. The numerical model is then validated.

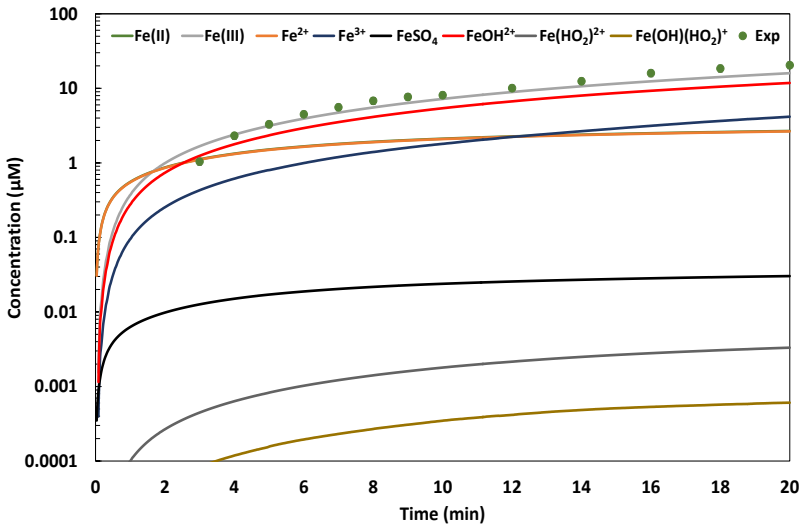

Figure 1. Evolution of Fe(III) concentration in experiment, and iron species concentrations obtained by simulation in function of time. Fe(II) and Fe^{2+} curves are superimposed because of the low $FeSO_4$ concentration. Concentration axis is in logarithmic scale

Hydroxyl Radical Production

Hydroxyl radical is characterized by the second highest redox potential after fluor, and has a non-selective character in terms of oxidized species. Advanced oxidation processes take advantage of both particularities of

hydroxyl radical to oxidize the organic molecules, notably the recalcitrant pollutant. In this part of the study, the validated numerical model is applied to simulate the evolution of the concentration of hydroxyl radical over 20 minutes of operation. The performance of the Galvano-Fenton degradation of pollutants, based on the generation of highly oxidative free radicals, principally $HO^{\bullet}$, is also compared to the performance of classic Fenton technique, considering a similar configuration and an initial concentration of added ferrous catalyst which is equivalent to the yield generated by galvanic corrosion over 20 min under the adopted conditions. Fig.2 reports these results in the presence of 2 µM of phenol.

This figure reveals that the kinetics of hydroxyl radical generation can be divided into two stages; the first stage would comprise the first 5 minutes starting from the beginning of the processes, while the second stage would correspond to the interval ranging from 5 to 20 min. During the first stage, the classic Fenton process results in a drastic increase of the concentration of $HO^{\bullet}$ in the electrolyte at the initial instant to the order of 10^{-8} mM. As soon as Fenton reagent and catalyst are added and put in contact, the rate of the H_2O_2 decomposition reaction strongly increases due to high concentrations of both reagent and catalyst. However, this scenario is only valid during the very beginning of the process, i.e., as long as the concentrations of H_2O_2 and Fe^{2+} are high. Once consumed, the concentration of H_2O_2 becomes limited, and the regeneration of Fe^{2+} becomes very slow, which inhibits the continuous release of $HO^{\bullet}$ during the second stage, and its concentration drops to less than 10^{-9} mM. Nevertheless, the high concentration of $HO^{\bullet}$ during the initial stage would strongly enhance the degradation process that would be decelerated afterward. In contrast, the Galvano-Fenton process is characterized by a quasi-linear increase of $HO^{\bullet}$ concentration during the first stage. At 5 min, it ends up at an order of magnitude of 10^{-9} mM. The concentration of $HO^{\bullet}$ continues its increase with the Galvano-Fenton process during the second stage and attains the highest concentration compared to the classic Feton process, with a value of 2.5×10^{-9} mM at 20 min.

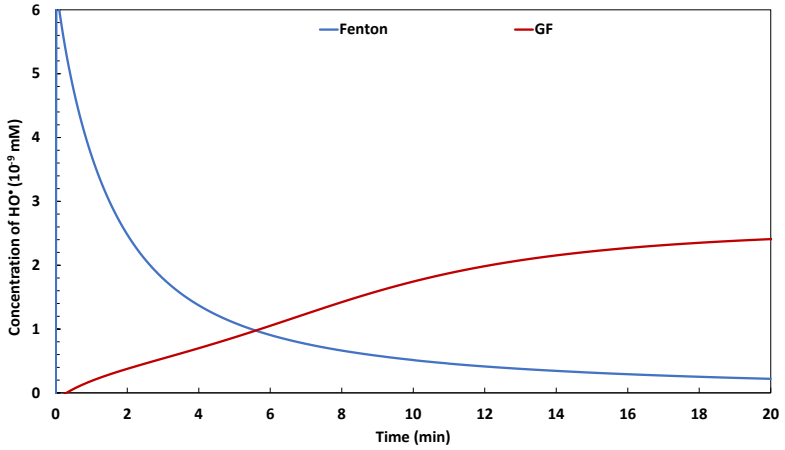

Figure 2. Evolutions of $HO^{\bullet}$ concentration in a function of time with classic Fenton and Galvano-Fenton processes in the presence of phenol at 2 µM.

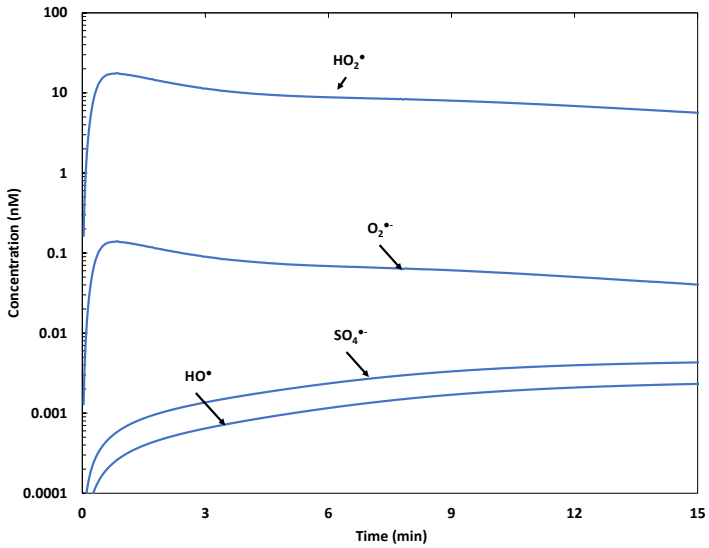

Figure 3. Analysis of the Galvano-Fenton technique in terms of the concentrations of free radicals.

We suggest inspecting the kinetics of the production of free radicals, namely, $HO^{\bullet}$, $HO_2^{\bullet}$, $SO_4^{\bullet-}$, and $O_2^{\bullet-}$, through the Galvano-Fenton process. Fig.3 reports the simulation results considering the addition of hydrogen peroxide at the initial time. The concentration of $HO^{\bullet}$ is quasi-null at t_0. The highest concentration among the four aforementioned free radicals is reached by $HO_2^{\bullet}$. At the initial instant, its concentration is about 0.2 nM at the addition of the hydrogen peroxide. In terms of molar yields, $HO_2^{\bullet}$ remains the free radical with the highest concentration within the electrolyte, followed by $O_2^{\bullet-}$, then $SO_4^{\bullet-}$ and finally $HO^{\bullet}$. This is due to the high reactivity of hydroxyl radical, making its lifetime within the electrolyte very short and its instantaneous concentration relatively low.

Degradation of Phenol

In the presence of an organic molecule, the hydroxyl radical produced by the Galvano-Fenton process is expected to provoke an oxidative attack initiating a decomposition process. With phenol, this mechanism is susceptible to lead to complete mineralization, as described in Table 2. In this part of the study, the evolution of phenol's concentration in function of time starting from an initial concentration of 2 µM is tracked and reported in Fig.4.

The Galvano-Fenton process shows a null initial degradation rate of phenol, revealed by the horizontal tangent of the curve of concentration of phenol vs. time. This observation is explained by the absence of the ferrous ion catalyst at t_0. However, this lasts a few seconds, then the phenol concentration starts decreasing linearly between 0.5 and 6 min. The phenol concentration reaches then 0.5 µM, which is equivalent to 75% degradation. The linear evolution of the phenol degradation through the Galvano-Fenton process occurs in parallel to the linear increase of the hydroxyl radical concentration, resulting from the gradual release of Fe^{2+} in the electrolyte through galvanic corrosion. The achievement of a degradation rate exceeding 96% requires almost 12 min. The initial latency, due to the absence of the Fenton catalyst when the process is started, is probably the reason for the delay observed in terms of the performance of the Galvano-Fenton process for the degradation of phenol.

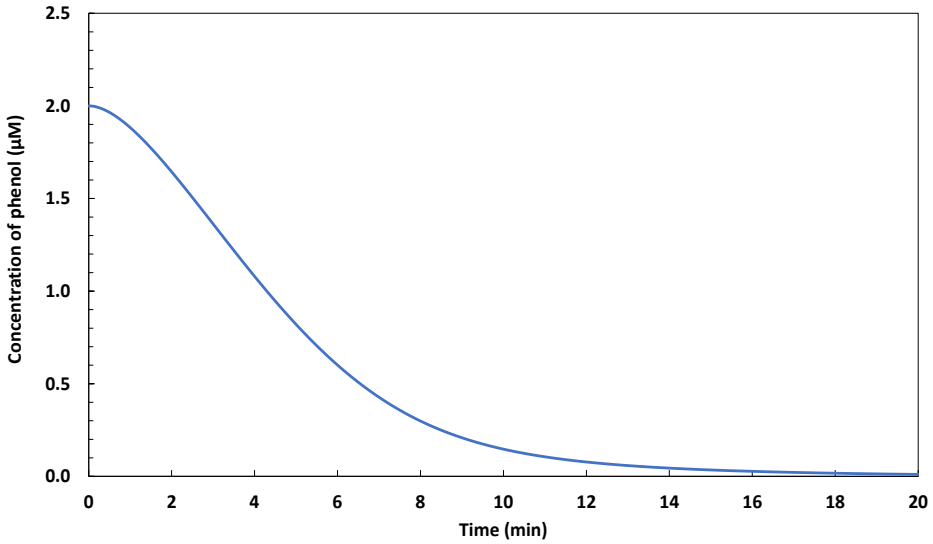

Figure 4. Evolution of the concentration of phenol in function of time with Galvano-Fenton process with an initial phenol concentration of 2 µM.

The mechanism of phenol degradation, which has been adopted in a previous work of our research group (Kerboua et al. 2021), is closely dependent on the release of free radicals in the electrolyte; hence, in Fig.5, we examine the evolution of the concentration of the intermediate species formed during phenol degradation using Galvano Fenton process, as described in Table 2. We notice that the concentration of the phenyl radical gradually increases in the case of the Galvano-Fenton process until it reaches a maximum value of 1.7 nM at 3 min. The same delay is observed in the evolution of the concentrations of the other intermediate species. For instance, the peak of the hydroxyphenyl radical concentration is observed at 3.6 min in the Galvano-Fenton process. Similarly, the maximum concentration of benzoquinone is reached at 5.5 min. The early apparition of the intermediate phenol degradation species reveals the most rapid degradation of phenol tending to its mineralization.

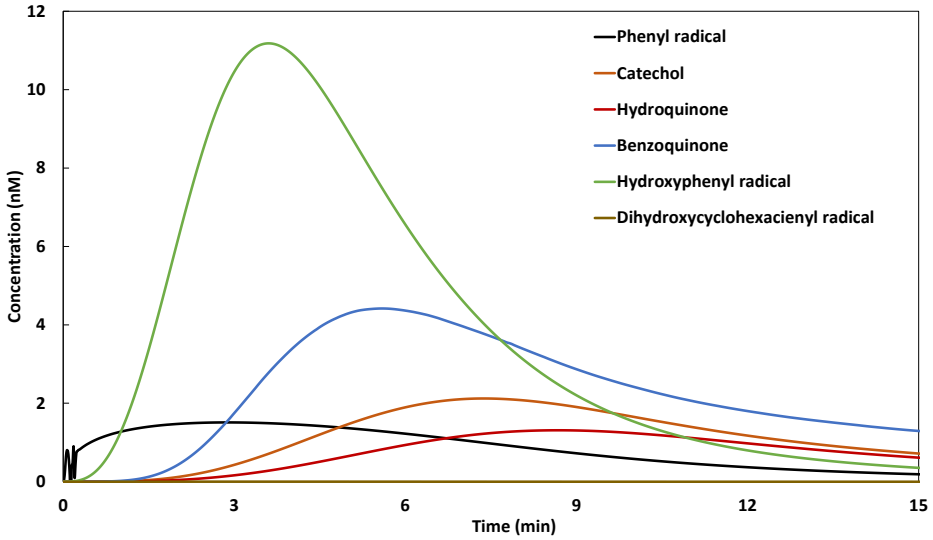

Figure 5. Kinetics of the formation of intermediate species from the degradation of phenol in the Galvano-Fenton process

Energetic Performance of the Technique

At present, we suggest relating the efficiency of the Galvano-Fenton to the energy release (Gasmi et al. 2021), compared to the efficiency of the electro-Fenton process to the energy consumption, considering similar conditions of spontaneous and forced electrochemical reactions. The polarization curves of the Fe-Cu galvanic cell within the Galvano-Fenton process with the configuration described earlier showed that the corrosion current is estimated at 298.75 µA for a corrosion potential of 0.277 V, which is equivalent to a maximum power of 82.75 mW. Considering an operating duration of 20 min, the total energy released by both configurations of the Galvano-Fenton process starting from the instant of the addition of H_2O_2would be to the order of 110.33 J.

In Fig.6, the ratios of the yield of hydroxyl radicals emerging over the process duration to the energy released by the Galvano-Fenton process is presented. In the same figure, we report the ratio of the yield of the produced hydroxyl radical in the electro-Fenton process, reported to the energy consumption using the same process. Conventionally, the energy release is expressed negatively. The figure demonstrates that with the Galvano-Fenton process, the ratio is estimated to be at 0.0311 nM per released Joule. On the opposite hand, an electro-Fenton process operating at the same conditions would produce 0.0059 nM per consumed Joule.

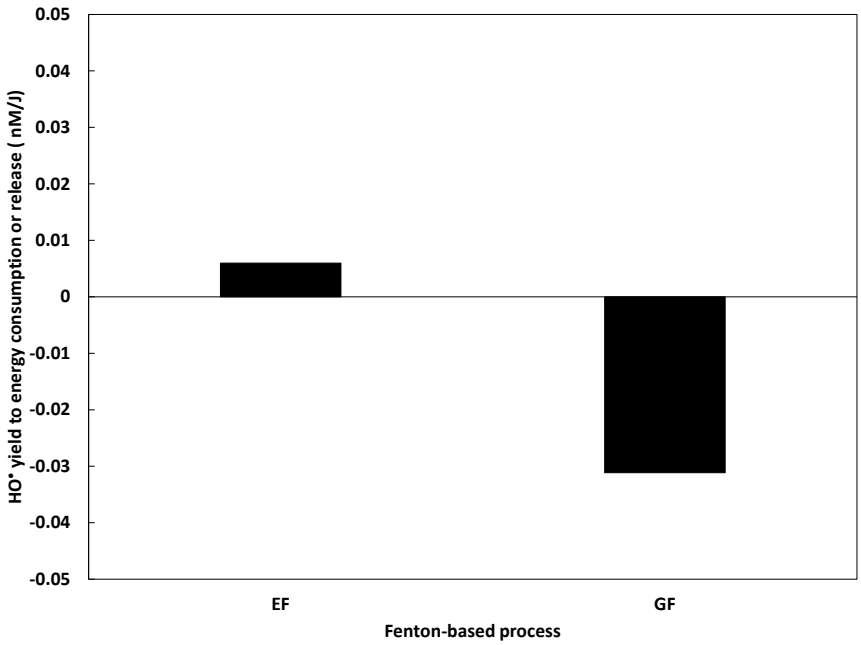

Figure 6. Ratios of the HO• yield to the consumed or released energy using Galvano-Fenton and Electro-Fenton processes.

In terms of phenol degradation efficiency, Fig.7 reports the ratio of the percentage of phenol degradation to the released or consumed energy when considering an initial phenol concentration of 2 µM. This figure shows that the Galvano-Fenton process can degrade 1.32% the initial phenol concentration by for each released Joule. The electro-Fenton process, however, would degrade 1.05% for each consumed joule. Overall, the Galvano-Fenton process, when treated as energetic systems, is characterized by a higher performance added to an energy release, in contrast, electro-Fenton process shows a lower performance and is associated with an energy consumption.

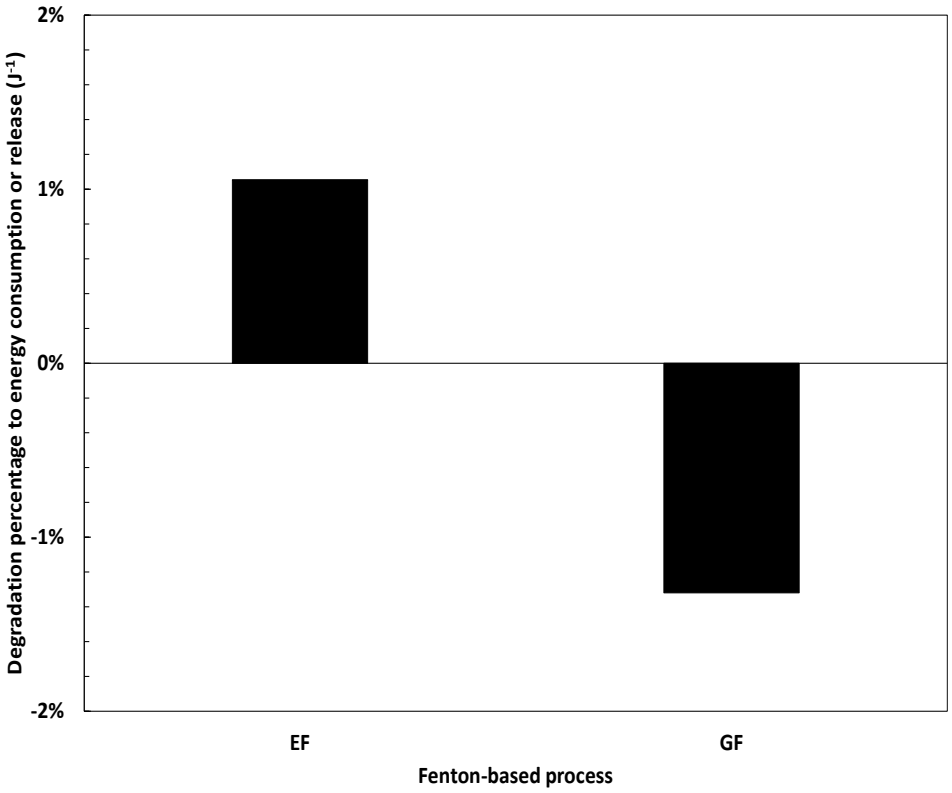

Figure 7. Ratios of phenol degradation percentage to the consumed or released energy using Galvano-Fenton and Electro-Fenton processes.

Conclusion

The mechanistic scenario considering no anodic regeneration of Fe2+ from Fe3+, and accounting for sulfate ions reactivity and iron complex formation showed a high correlation with experimental results of 93.5%. The concentration of $HO^{\bullet}$ continues its increase with the Galvano-Fenton process during the second stage and attains the highest concentration compared to Fenton, with a value of 2.5×10^{-9} mM at 20 min.

In terms of molar yields, $HO_2^{\bullet}$ remains the free radical with the highest concentration within the electrolyte, followed by $O_2^{\bullet-}$, then $SO_4^{\bullet-}$ and finally $HO^{\bullet}$. Hydroxyl radical shows the lowest concentration because of its high reactivity, making its lifetime within the electrolyte very short and its instantaneous concentration relatively low.

The achievement of a phenol degradation rate exceeding 96% requires almost 12 min. The initial latency, due to the absence of the Fenton catalyst when the process is started, is probably the reason for the delay observed in terms of the performance of the Galvano-Fenton process for the degradation of phenol. In terms of the mechanism concerns of phenol degradation, the early apparition of the intermediate species reveals the rapid degradation of phenol tending to its mineralization.

Overall, the Galvano-Fenton process, when treated as energetic systems, is characterized by a higher performance added to an energy release, in contrast, electro-Fenton process shows a lower performance and is associated with an energy consumption.

Scientific Ethics Declaration

The authors declare that the scientific ethical and legal responsibility of this article published in EPSTEM journal belongs to the authors.

Acknowledgements

* This article was presented as an oral presentation at the International Conference on Technology, Engineering and Science (www.icontes.net) held in Antalya/Turkey on November 16-19, 2022.

* This work was financially supported by the "Hubert Curien Program" through the PHC MAGHREB Project number 19MAG23/41382WC, the Deep Tech Innovation Incubator of Lyon and Saint-Etienne PULSALYS and the Deanship of Scientific Research at King Saud University through research group No. RG-1441-501.

References

Ahmad, Z. (2006). Corrosion kinetics. In Zaki B. T. (Ed.), *Principles of corrosion engineering and corrosion control*, (pp. 57–119) Oxford: Butterworth-Heinemann,). https://www.sciencedirect.com/science/article/pii/B9780750659246500040.

Andreozzi, R., Antonio D. A., & Raffaele M. (2000). A kinetic model for the degradation of benzothiazole by Fe3+ -photo-assisted fenton process in a completely mixed batch reactor. *Journal of Hazardous Materials*, *80*: 241–57.

Artusi, R., Verderio, P., & Marubini, E. (2002). Bravais-Pearson and Spearman correlation coefficients: Meaning, test of hypothesis and confidence ınterval. *International Journal of Biological Markers 17*(2): 148–51.

Bray, W. C. (1931). The mechanism of reactions in aqueous solution examples involving equilibria and steady states. *Chemical Reviews*, *X*(1): 161–77.

Davis, M. E. & Davis, M. E., & Robert J. D. (2003). The basics of reaction kinetics for chemical reaction engineering. In Davis, R. J. (Ed). *Fundamentals of chemical reaction engineering*, New York: McGraw Hill, 1–52. http://resolver.caltech.edu/CaltechBOOK:2003.001.

De Laat, J., & Gallard, H. (1999). Catalytic decomposition of hydrogen peroxide by fe(ıı) in homogeneous aqueous solution: Mechanism and kinetic modeling. *Environmental Science and Technology*, *33*(16): 2726–32.

Duesterberg, C. K., & Waite, T. D. (2006). Process optimization of fenton oxidation using kinetic modeling. *Environmental Science and Technology*, *40*(13): 4189–95.

Gasmi, I., Kerboua, K., Haddour, N., Hamdaoui, O., Alghyamah, A., & Buret, F. (2020). Kinetic pathways of ıron electrode transformations in Galvano-Fenton process: A mechanistic ınvestigation of in-situ catalyst formation and regeneration. *Journal of the Taiwan Institute of Chemical Engineers*, *116*, 81–91.

Gasmi, I., Haddour, N., Hamdaoui, O., Kerboua, K., Alghyamah, A., & Buret, F. (2021). A novel energy-from-waste approach for electrical energy production by galvano – Fenton Process. *Molecules*, 26(4013), 1–14.

Haag, W. R., & Yao, C. D. (1992). Rate constants for reaction of hydroxyl radicals with several drinking water contaminants. *Environmental Science and Technology*, *26*(5), 1005–13.

Haber, F., & Weiss, J. (1932) The catalytic decomposition of hydrogen peroxide by ıron salts. *Proceedings of the Royal Society of London. Series A, Mathematical and Physical Sciences*, *147*(861), 332–51.

Machulek Jr, A., Quina, F. H., Gozzi, F., Silva, V. O., Friedrich, L. C., & Moraes, J. E. (2012). Fundamental mechanistic studies of the photo-fenton reaction for the degradation of organic pollutants. In *Organic Pollutants Ten Years After the Stockholm Convention - Environmental and Analytical Update*, , 272–92.

Kerboua, K., Hamdaoui, O., Haddour, N., & Alghyamah, A. (2021). Simultaneous galvanic generation of Fe2+ catalyst and spontaneous energy release in the Galvano-Fenton Technique : A numerical ınvestigation of phenol's oxidation and energy production and saving. *Catalysts* 11(943).

Kušić, H., Koprivanac, N., Božić, A. L., & Selanec, I. (2006).Photo-assisted fenton type processes for the degradation of phenol : A kinetic study. *Journal of Hazardous Materials*, *136*, 632–44.

Liochev, S. I., & Fridovich, I. (2002). The Haber-Weiss cycle—70 years later: an alternative view. *Redox Report*, *7*(1), 55-57.

Lower, S. K. (2004). Chemical reactions at an electrode, galvanic and electrolytic cells. *Electrochemistry. Simon*

Fraser University, 35-38.
Lu, M., Wang, J., Wang, Y., & He, Z. (2021). Heterogeneous photo-fenton catalytic degradation of practical pharmaceutical wastewater by modified attapulgite supported multi-metal oxides. *Water*, *13*(2), 156.
Machulek, A., Moraes, J. E. F., Okano, L. T., Silvérioc, C. A., & Quina, F. H. (2009). Photolysis of ferric ions in the presence of sulfate or chloride ions: implications for the photo-Fenton process. *Photochemical & Photobiological Sciences*, *8*(7), 985-991.
Madhavan, J., Grieser, F., & Ashokkumar, M. (2010). Combined advanced oxidation processes for the synergistic degradation of ibuprofen in aqueous environments. *Journal of Hazardous Materials*, *178*(1-3), 202-208. http://dx.doi.org/10.1016/j.jhazmat.2010.01.064.
Martins, A. F., Wilde, M. L., Vasconcelos, T. G., & Henriques, D. M. (2006). Nonylphenol polyethoxylate degradation by means of electrocoagulation and electrochemical Fenton. *Separation and Purification Technology*, *50*(2), 249-255.
Merouani, S., Hamdaoui, O., Saoudi, F., & Chiha, M. (2010). Influence of experimental parameters on sonochemistry dosimetries: KI oxidation, Fricke reaction and H2O2 production. *Journal of Hazardous Materials*, *178*(1-3), 1007-1014.
Monteil, H., Pechaud, Y., Oturan, N., & Oturan, M. A. (2019). A review on efficiency and cost effectiveness of electro-and bio-electro-Fenton processes: Application to the treatment of pharmaceutical pollutants in water. *Chemical Engineering Journal*, *376*, 119577.. https://doi.org/10.1016/j.cej.2018.07.179.
Pawar, V. & Sagar G. (2015). An overview of the fenton process for ındustrial wastewater. *IOSR Journal of Mechanical and Civil Engineering (IOSR-JMCE)*: 127–36.
Shokri, A. (2018). Application of Sono–photo-Fenton process for degradation of phenol derivatives in petrochemical wastewater using full factorial design of experiment. *International Journal of Industrial Chemistry*, *9*(4), 295-303.
Shreir, L. L, Jarman R. A., & Burstein G. T. (1994). 2 Butterworth-Heinemann *Corrosion Control*.
Tarkwa, J. B., Oturan, N., Acayanka, E., Laminsi, S., & Oturan, M. A. (2019). Photo-Fenton oxidation of Orange G azo dye: process optimization and mineralization mechanism. *Environmental Chemistry Letters*, *17*(1), 473-479. https://doi.org/10.1007/s10311-018-0773-0.
Xu, L. J., Chu, W., & Graham, N. (2014). Degradation of di-n-butyl phthalate by a homogeneous sono–photo–Fenton process with in situ generated hydrogen peroxide. *Chemical Engineering Journal*, *240*, 541-547.
Zhang, M. H., Dong, H., Zhao, L., Wang, D. X., & Meng, D. (2019). A review on Fenton process for organic wastewater treatment based on optimization perspective. *Science of the Total Environment*, *670*, 110-121.Wastewater Treatment Based on Optimization Perspective." *Science of the Total Environment* 670: 110–21.

Author Information

Kaouther Kerboua
Department of Engineering, Higher School of Industrial Technologies
PO box 2018, 23000, Annaba, Algeria
Contact e-mail: *k.kerboua@esti-annaba.dz*

Naoufel Haddour
Laboratoire Ampère, Ecole Centrale de Lyon
36 Avenue Guy de Collongue, 69134, Ecully, France

Intissar Gasmi
Laboratory of Environmental Engineering, Process Engineering Department, Faculty of Engineering, Badji Mokhtar - Annaba University,
P.O. Box 12, 23000, Annaba, Algeria
Laboratoire Ampère, Ecole Centrale de Lyon
36 Avenue Guy de Collongue, 69134, Ecully, France

Oualid Hamdaoui
Chemical Engineering Department, College of Engineering, King Saud University
P.O. Box 800, 11421 Riyadh, Saudi Arabia

To cite this article:

Kerboua, K., Haddour, N., Gasmi, I. & Hamdaoui, O. (2022). Water remediation from recalcitrant pollution using the galvano-fenton process: a modeling approach of the hydroxyl radical generation and the energy efficiency. *The Eurasia Proceedings of Science, Technology, Engineering & Mathematics (EPSTEM), 21,* 506-516.